iScience

CellPress
OPEN ACCESS

Article

Proteomic pathways to metabolic disease and type 2 diabetes in the pancreatic islet

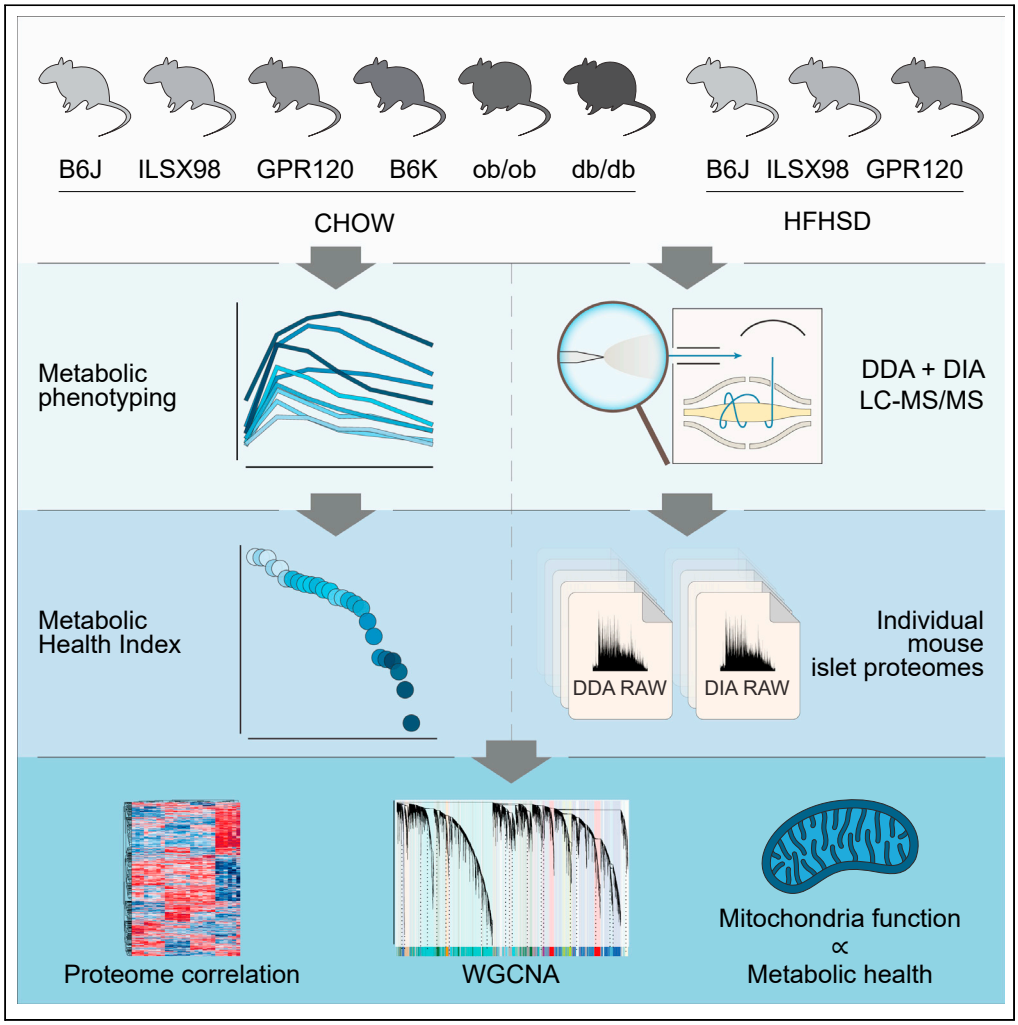

Belinda Yau, Sheyda Naghiloo, Alexis Diaz-Vegas, ..., David E. James, Sean J. Humphrey, Melkam A. Kebede

sean.humphrey@sydney.edu.au (S.J.H.)
melkam.kebede@sydney.edu.au (M.A.K.)

Highlights

Most comprehensive mouse islet proteome library generated to date

Quantification of islet proteomic changes across 6 strains of mice on 2 diets

Islet mitochondrial function revealed as strain-independent regulator of metabolic health

Yau et al., iScience *24*, 103099
October 22, 2021
https://doi.org/10.1016/j.isci.2021.103099

iScience

CellPress
OPEN ACCESS

Article

Proteomic pathways to metabolic disease and type 2 diabetes in the pancreatic islet

Belinda Yau,[1,8] Sheyda Naghiloo,[1,8] Alexis Diaz-Vegas,[3] Austin V. Carr,[2] Julian Van Gerwen,[3] Elise J. Needham,[3] Dillon Jevon,[1] Sing-Young Chen,[5] Kyle L. Hoehn,[5,6] Amanda E. Brandon,[1] Laurance Macia,[1] Gregory J. Cooney,[1] Michael R. Shortreed,[2] Lloyd M. Smith,[2] Mark P. Keller,[4] Peter Thorn,[1] Mark Larance,[3] David E. James,[1,3] Sean J. Humphrey,[3,*] and Melkam A. Kebede[1,7,9,*]

SUMMARY

Pancreatic islets are essential for maintaining physiological blood glucose levels, and declining islet function is a hallmark of type 2 diabetes. We employ mass spectrometry-based proteomics to systematically analyze islets from 9 genetic or diet-induced mouse models representing a broad cross-section of metabolic health. Quantifying the islet proteome to a depth of >11,500 proteins, this study represents the most detailed analysis of mouse islet proteins to date. Our data highlight that the majority of islet proteins are expressed in all strains and diets, but more than half of the proteins vary in expression levels, principally due to genetics. Associating these varied protein expression levels on an individual animal basis with individual phenotypic measures reveals islet mitochondrial function as a major positive indicator of metabolic health regardless of strain. This compendium of strain-specific and dietary changes to mouse islet proteomes represents a comprehensive resource for basic and translational islet cell biology.

INTRODUCTION

Type 2 diabetes (T2D) is characterized by sustained hyperglycaemia. Left uncontrolled it may lead to complications such as retinopathy, neuropathy, nephropathy, and increased risk of cardiovascular disease and stroke (Antonetti et al., 2021); Harding et al. (2019). Prior to T2D onset, whole-body insulin resistance is balanced by compensatory increases in insulin production and secretion by the pancreatic β-cells to maintain euglycaemia (Hudish et al., 2019). Although the mechanisms involved in β-cell compensation are not fully understood, islet mass expansion and increased β-cell function are known to be important (Clark et al., 2001). In some cases however, islets eventually fail to maintain sufficient insulin output by this compensatory mechanism, leading to overt hyperglycaemia and T2D (Kahn, 2003). Despite the importance of β-cell failure in the etiology of T2D, the molecular mechanisms underpinning islet dysregulation remain poorly understood.

Both cellular and environmental factors contribute to the pathogenesis of T2D. While insulin resistance is believed to be primarily caused by environmental factors such as overnutrition and a sedentary lifestyle, the ability of the pancreatic islets to compensate is heavily influenced by genetics (Liu et al., 2021). Indeed, most of the genes identified by genome-wide association studies in human T2D are genes that control β-cell function and mass (Groop and Lyssenko, 2009). Identifying the changes in islet function during the transition from compensation to failure is therefore key to understanding the pathogenesis of T2D (Alarcon et al., 2016; Kang et al., 2019, 2020; Keller et al., 2019). Since proteins are the biochemical machinery of the cell, phenotypes typically emerge at the level of the proteome. Analyzing the proteome of islets from different species and insulin-resistant models that either compensate for insulin resistance or progress to T2D therefore promises to reveal key molecular contributors to this process. This study aims to investigate the relationship between whole-body metabolic health and the pancreatic islet, using mouse models that exhibit a range of insulin resistance or progression to T2D as a reflection of environmental and genetic diversity. Our goal is to reveal key molecular contributors to T2D pathogenesis independent of just a single genetic background and uncover physiological pathways that may be relevant to broader metabolic health. Accordingly, we performed an unbiased quantitative proteomic analysis of islets isolated from animal models of obesity/insulin resistance (spontaneous and dietary-induced) that display a broad range of susceptibility to metabolic abnormalities and T2D.

[1]Discipline of Physiology, School of Medical Sciences, Charles Perkins Centre, University of Sydney, Camperdown 2006, Australia

[2]Department of Chemistry, University of Wisconsin-Madison, Madison, WI, USA

[3]School of Life and Environmental Sciences, Faculty of Science, The University of Sydney, Sydney, NSW, Australia

[4]Department of Biochemistry, University of Wisconsin-Madison, Madison, WI, USA

[5]Department of Biotechnology and Biomolecular Sciences, University of New South Wales, Kensington, NSW 2052, Australia

[6]Department of Pharmacology, University of Virginia, Charlottesville, VA 22908, USA

[7]Senior author

[8]These authors contributed equally

[9]Lead contact

*Correspondence: sean.humphrey@sydney.edu.au (S.J.H.), melkam.kebede@sydney.edu.au (M.A.K.)

https://doi.org/10.1016/j.isci.2021.103099

We performed deep proteome profiling of islets isolated from each mouse and across multiple strains and diets, enabling the correlation of islet function with proteomic changes to gain insights into key functional nodes for metabolic health. From two independent analyses, islet mitochondrial function emerged as a significant indicator of healthy metabolic status, negatively correlating with increased fasting insulin, increased fat mass and impaired glucose tolerance.

RESULTS

Genetic and dietary mouse models of islet function

In total, we studied nine different genetic or dietary mouse models. Two of these were "spontaneous" models – the diabetic *db/db* mouse and the insulin-resistant *ob/ob* mouse. Despite both genetic mutations in these strains resulting in altered leptin signaling, the *db/db* mouse is susceptible to developing T2D due to its C57BL/6K genetic background, while the *ob/ob* strain on the C57BL/6J background is not. As such, while both models display obesity, glucose intolerant and hyperinsulinemic phenotypes, only the *db/db* mouse eventually develops hyperglycaemia (Chen et al., 1996; Friedman and Halaas, 1998). Prolonged exposure of the C57BL/6J mouse to a high fat, high sucrose diet (HFHSD) likewise results in the development of obesity, hyperinsulinemia, and glucose-intolerance (Ahren and Scheurink, 1998; Surwit et al., 1988) but not T2D. Our HFHSD-fed strains included the C57BL/6J mouse, a whole-body free fatty acid receptor 4 (FFAR4), commonly referred to G protein-coupled receptor 120 (GPR120), knockout mouse (on the C57BL/6J genetic background), and the Inbred Long-Sleep x Inbred Short-Sleep – 98 (ILSxISS98) strain (Bennett et al., 2006; Williams et al., 2004).

GPR120 plays an important role in dietary fat sensing and in the control of energy balance in both humans and rodents (Ichimura et al., 2012). It is a receptor for medium- to long-chain fatty acids and is expressed in several tissues including small intestine (Hirasawa et al., 2005), adipocytes (Oh et al., 2010), immune cells (Oh et al., 2010), and in the pancreatic islets (Croze et al., 2021; Stone et al., 2014). GPR120 activation therefore regulates several processes including secretion of enteroendocrine hormones (Ichimura et al., 2012; Tanaka et al., 2008), adipogenesis (Gotoh et al., 2007; Ichimura et al., 2012; Oh et al., 2010), insulin sensitivity and inflammation (Oh et al., 2010). Although earlier studies reported a lack of GPR120 expression in whole pancreas or isolated islets (Hirasawa et al., 2005; Tanaka et al., 2008), recent studies have since confirmed an enrichment of GPR120 expression in delta-cells (Croze et al., 2021; Stone et al., 2014). Its activation in islets is reported to potentiate both glucagon secretion from alpha-cells (Suckow et al., 2014) and glucose-stimulated insulin secretion from β-cells (Moran et al., 2014) while inhibiting glucose-stimulated somatostatin secretion from delta-cells (Croze et al., 2021; Stone et al., 2014), and therefore contribute to the regulation of glucose homesostasis.

Although the ILSxISS98 strain has not previously been assessed in terms of its metabolic parameters in response to HFHSD feeding, its closest family member ILSxISS97 is resistant to HFHSD-induced metabolic abnormalities (Stockli et al., 2017). Both strains were shown to have decreased life span on a calorie restricted diet (Liao et al., 2010). As an inbred strain originally derived by selection from an 8-way heterogeneous stock selected for differential sensitivity to sedative effects of ethanol, ILSxISS98 was selected in particular to increase the overall genetic diversity of the panel and investigate how these mice handle an excessive nutrient environment with HFHSD to uncover insights into potential protective mechanisms.

In vivo and *ex vivo* phenotypic variation across mouse strains and HFHSD intervention

We performed detailed *in vivo* metabolic and *ex vivo* islet measurements to obtain detailed phenotypic profiles of our models. In total we studied twenty-six mice, comprising six strains on a standard CHOW diet, and three strains (C57BL/6J, ILSxISS98 and GPR120 KO) that were also placed on an HFHSD at 8 weeks of age for an 8-week duration (STAR Methods). At 14–15 weeks of age, body composition was analyzed by EchoMRI, and mice were fasted for 6 h prior to blood glucose measurements during an intraperitoneal glucose tolerance test (ipGTT). Blood insulin levels were also collected at fasting and 15 min after glucose administration. Pancreatic islets were isolated at 15–16 weeks of age and 30 islets per mouse were used to assess *ex vivo* islet function by glucose-stimulated insulin secretion assay, and insulin content measurements. The remainder of the islets was utilized for proteomic analysis.

Average mouse weight was 34.45 ± 9.4 g, with weight gain in HFHSD-fed C57BL/6J and ILSxISS98 ($p < 0.05$), and *db/db* mice ($p < 0.01$), attributed to significant fat-mass gain compared to their CHOW and genetic counterparts, respectively (Figure 1A). Across all individual mice except one CHOW-fed *db/db* mouse

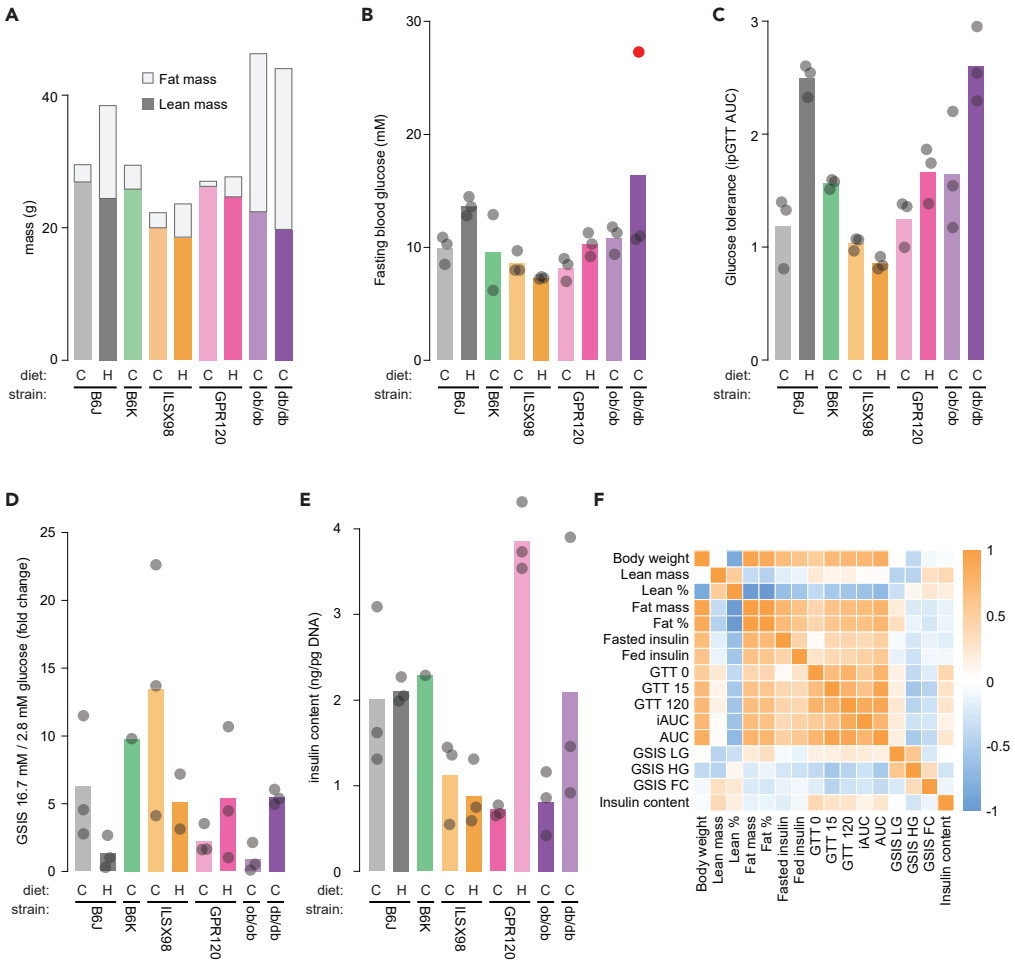

Figure 1. *In vivo* and *ex vivo* islet phenotyping of mouse strain panel

(A) Body weight measurements determined by echoMRI for total mass, and lean and fat mass composition.

(B) Blood glucose levels after 5 h fast. Red datapoint indicates *db/db* diabetic mouse.

(C) Total area under the curve of blood glucose levels during an intraperitoneal glucose tolerance test.

(D) Fold change of insulin secretion in media measured from a glucose-stimulated insulin secretion assay from overnight-recovered islets stimulated at 2.8 mM and 16.7 mM glucose.

(E) Total islet insulin content in islets normalized to total islet DNA content.

(F) Correlation of all measured phenotypic traits in individual mice; *in vivo* body composition, blood glucose and blood insulin and *ex vivo* islet glucose-stimulated insulin secretion, total insulin content, and percentage insulin secretion. All *in vivo* phenotyping was performed at 14–15 weeks (A–C) and *ex vivo* phenotyping was measured at 15–16 weeks. Data is presented as mean.

(red circle), fasting glucose was well-maintained at a physiologically healthy range, although C57BL/6J mice had higher fasting glucose on HFHSD compared to their CHOW counterparts ($p < 0.05$) (Figure 1B). Glucose tolerance testing also further illustrated the large variation in metabolic outcomes across strains (Figure S1A), with significant increases in AUC in both C57BL/6J and GPR120 KO HFHSD-fed mice compared to their CHOW counterparts ($p < 0.01$, Figure 1C). Surprisingly, ILSxISS98 mice had improved glucose tolerance in HFHSD-fed mice, compared with CHOW-fed mice ($p < 0.05$, Figure 1C). Whole-body insulin measurements, both fasting and fed (15 min post a glucose bolus during the GTT) similarly demonstrated strain and diet variations, with notably higher values observed in *db/db* mice (Figure S1B).

Basal insulin secretion at 2.8 mM glucose in *ex vivo* islets from HFHSD-fed C57BL/6J mice was significantly higher compared to their CHOW controls, resulting in decreased fold change of insulin secretion when the islets were further stimulated with 16.7 mM glucose ($p < 0.05$, Figures S1C and 1D). Total islet insulin content, normalized to total islet DNA, also reflected substantial variation between strains, with a range of

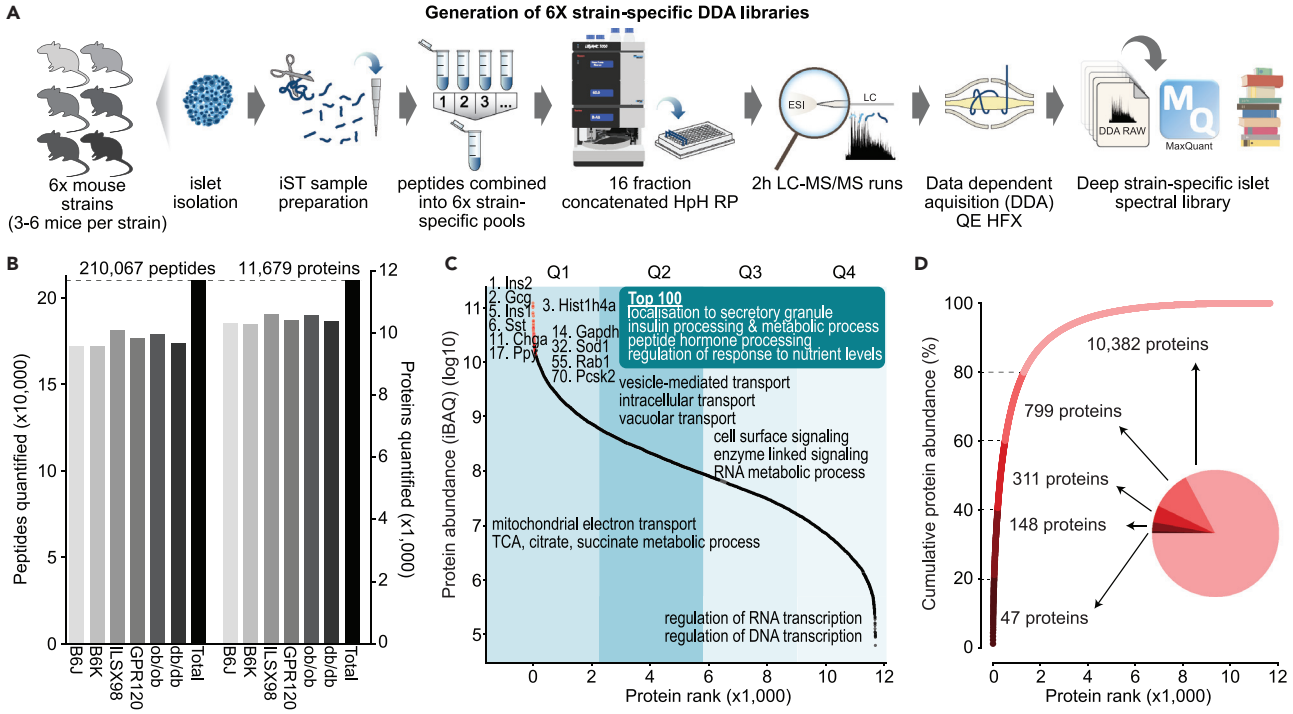

Figure 2. Measurement of deep strain-specific islet proteome libraries

(A) Schematic of the workflow used to generate the strain-specific islet proteomes.

(B) Unique peptides and proteins quantified in islets from each of the strains.

(C) Median intensity-based absolute quantification (iBAQ) values of the mouse islet proteome libraries. Proteins were stratified into quartiles, and annotated for Gene Ontology terms significantly enriched in each quartile (Fisher exact test, Benj.-Hochberg FDR <0.02).

(D) Cumulative protein abundance of the ranked islet proteome.

0.42–4.31 ng insulin/pg DNA across all individual mice (Figure 1E). Correlation analyses performed between all measured phenotypes in our mice revealed correlations ($r \geq 0.4$) between *in vivo* metabolic measures, but poor correlations between *in vivo* phenotypes and islet-centric phenotypes (except for islet insulin content and glucose tolerance) (Figure 1F).

Generation of a deep strain-specific islet proteome library using DDA mass spectrometry

We reasoned that the generation of high-quality strain-specific islet proteome spectral libraries measured by data-dependent acquisition MS could be employed to maximize the coverage of individual mouse islet proteomes measured by data-independent MS, without the need to fractionate all individual samples. Thus, we first pooled islet proteins from 3–6 biological replicates of each strain, producing 6 different samples representing all genetic backgrounds. For these pooled strain islet samples, we fractionated peptides into 16 fractions by high pH reversed-phase chromatography (STAR Methods) and analyzed the samples by high-resolution liquid chromatography-mass spectrometry (LC-MS) on a benchtop Orbitrap ('Q Exactive HF-X') mass spectrometer in data-dependent format (Figure 2A). We analyzed these data using MaxQuant (Cox and Mann, 2008), generating a strain-specific library of islet peptides and associated spectra. In total, from our fractionated DDA measurements we quantified over 200,000 unique tryptic peptides, with more than 170,000 peptides quantified in each strain (Figure 2B). Together, this high peptide coverage enabled the quantification of 11,679 different islet proteins, with a median sequence coverage of >30% and 88–91% (10,284–10,612) of these proteins were found in each strain (Figure 2B, Data S1; Table S1). Previous human islet proteomic studies identified 3,365 and 4,594 proteins (Metz et al., 2006; Schrimpe-Rutledge et al., 2012), while the most extensive proteomic analysis of human islets to date (Nakayasu et al., 2020) identified 11,324 proteins using TMT-labeling and fractionation into 24 fractions. Due to the batching of samples required with TMT multiplexing, 85% (9,695 proteins) were identified in both experiments. Previous mouse islet proteomic studies have identified a range of 302–6,113 proteins (Mitok et al., 2018; Petyuk et al., 2008; Villafuerte et al., 2017; Wortham et al., 2018; Zhang et al., 2017). Thus, to our knowledge this strain-specific reference library represents the most comprehensive quantitative compendium of mouse islet peptides and proteins to date.

A ranked abundance atlas of islet protein expression

We next estimated the abundance of >11,000 proteins in the islet proteome using "intensity-based absolute quantification" (iBAQ) (Schwanhausser et al., 2011), generating a ranked abundance atlas of the islet proteome (Figure 2C, Data S1; Table S2). Insulin (*Ins2* and *Ins1*) was the most abundant protein, contributing ~2% of the total islet protein signal. The second most abundant protein was glucagon (*Gcg*), which is striking since α-cells in which glucagon is produced represent only 15–20% of islet cells by number. Similarly, somatostatin (*Sst*) and pancreatic polypeptide (*Ppy*), the primary secretory molecules of the δ- and PP-cells, representing fewer than 10% and 1% of islet cells respectively, were the 6th and 17th most abundant proteins in the bulk islet proteome. The abundance of these proteins amongst the islet proteome despite the relatively low population of the cell types in which they are produced emphasizes the relative importance of their secretory roles to islet function. The 47 most abundant islet proteins together contributed a cumulative 20% of the islet protein signal, while the remaining 80% of proteins collectively contributed only 20% of the measured protein abundance (Figure 2D). The "top 100" proteins were altogether enriched in *insulin metabolic processes*, *insulin processing* and *peptide processing* pathways, as well as *protein localization to secretory granule*. This again reflects the importance of the secretory pathway to the overall identity of the pancreatic islet as a mini-organ. To explore enrichment of protein functional classes throughout the islet proteome from the perspective of abundance, we further stratified islet proteins by protein abundance into quartiles (Q1 to Q4, high to low abundance) and assessed each for the enrichment of protein function. In Q1, *mitochondrial electron transport*, *TCA and citrate metabolic processes* and *respiratory electron chain transport* pathway enrichment highlight the importance of glucose oxidation to islet function, while Q2 enrichment of annotations including *cellular localization, vesicle-mediated transport,* and *intracellular transport* reiterate the significance of secretory vesicle trafficking in the endocrine organ (Figure 2C). Q3-Q4 were enriched in proteins from cell surface receptor signaling pathways as well as various RNA processes and transcriptional regulators, suggesting that the expression of these proteins may be finely tuned from a lower level. This ranked compendium of islet protein abundance should serve as a useful reference for the proteomic and islet biology fields (Data S1; Table S2).

Individual mouse islet proteomes using DIA mass spectrometry

We next analyzed all islet proteomes in unfractionated single-run format, operating the mass spectrometer in data-independent acquisition (DIA) mode (Chapman et al., 2014). We analyzed these proteome data from islets obtained from 26 individual mice across 9 strain/diet combinations and utilized our MaxQuant-generated deep islet-specific spectral library to facilitate peptide identification (Figure 3A). This strategy enabled us to reliably quantify in total 8,673 islet proteins, with over 8,000 of these found in every individual mouse islet proteome (Figure 3B). In each diet or genetic model studied, we quantified between 93 and 95% of the total islet proteins (8,058–8,234 proteins), revealing that almost all islet proteins are expressed in each mouse. This suggests that islet proteome variation exists primarily at the level of protein abundance, rather than unique expression of new proteins.

Our individual mouse islet proteome data were highly accurate and reproducible, with Pearson correlation coefficients between strains >0.92, and correlation across all islet samples >0.88 (Figure 3C). Median coefficients of variation from proteins across 3 biological replicates in each group are reported in Figure S2. An unsupervised PCA analysis demonstrated clear grouping of samples by strain, suggesting that the majority of variance between samples can be attributed to their genetic background, rather than diet (Figure 3D), although diet could be separated by component 1 in PCA analysis of individual strains (Figure S3). Both *ob/ob* and *db/db* CHOW mice also showed clear separation from the other strains in the first component, suggesting that these two extremes in metabolic health could also be clearly differentiated by their islet proteomes.

We next analyzed the expression of all proteins across all 26 islet proteomes, and found that over 50% of the islet proteome (4,932 proteins) were differentially abundant (ANOVA, FDR <0.05). A similar proportion was regulated when comparing only those strains with diet comparisons (47%, 3,937 proteins, two-way ANOVA, FDR <0.05). In those strains, 25% (2,042 proteins) of the proteome was specifically regulated by the HFD in at least one strain.

A complete list of these proteins and their regulation by strain or diet are provided in Data S1; Tables S3–S5. Individual group comparisons, between strains or diet, allow identification of significantly regulated

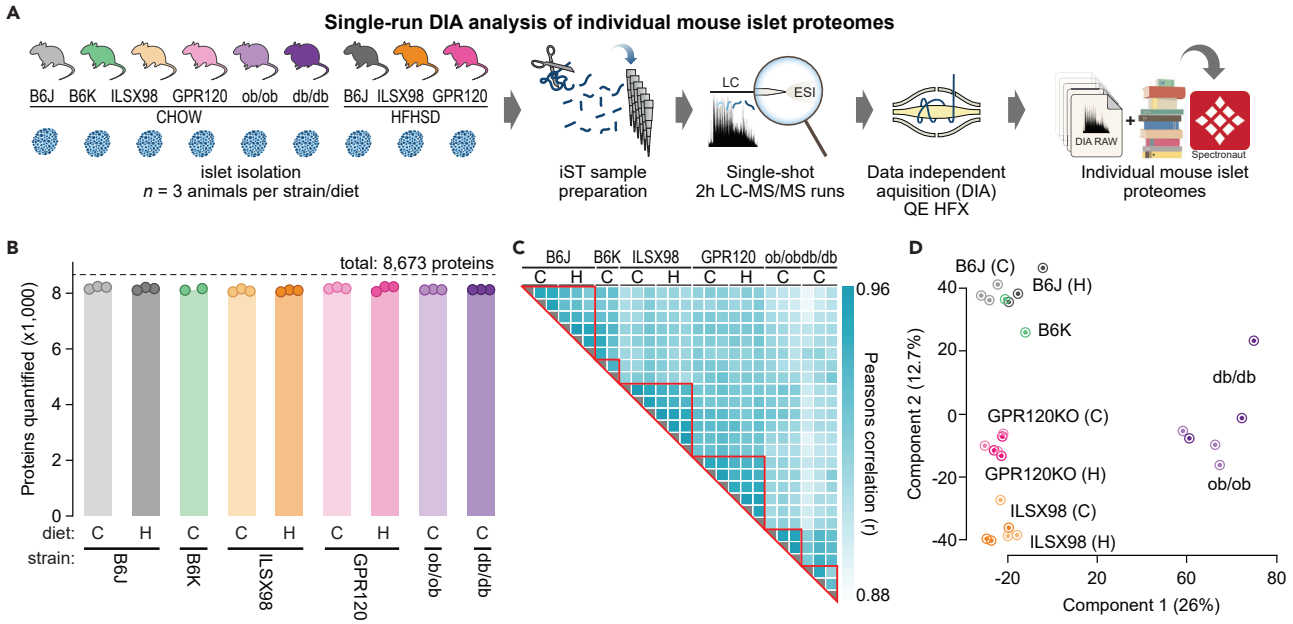

Figure 3. Proteomes of individual mouse islets at 15–16 weeks of age

(A) Schematic of the workflow used to generate the individual mouse islet proteomes.

(B) Number of unique identified proteins in individual mice. Dotted line indicates total unique proteins identified across all islet proteomes, columns are presented as mean.

(C) Pearson correlation of all individual mouse islet proteomes.

(D) Unsupervised PCA clustering of individual mouse islet proteomes.

proteins between each diet and strain (Welch's t test, FDR <0.05, $q < 0.05$, Figure S4) and provide a valuable public resource for islet interrogation (https://kebedelab.com/islet-proteome-resource).

Unsupervised hierarchical clustering of the islet proteome further revealed groups predominantly divided by strain, followed by diet (Figure 4A). We selected major clusters and assessed enrichment of specific groups of proteins using Gene Ontology (GO) annotated pathways (Figure 4B). This identified reduced expression of mitochondrial respiratory chain complex III, TCA cycle, and oxidative phosphorylation proteins in *ob/ob* and *db/db* strains, while proteasomal and ribosomal proteins were elevated in the same strains. Mitochondrial respiratory chain complex I proteins were also lower in the ILSxISS98 strain. Together, these data suggest that the expression of key protein groups within the pancreatic islet classify and characterize specific strains.

Association of islet proteome with metabolic phenotype

To enable characterization of islet proteins that may contribute to whole-body metabolic function, we next established a weighted "metabolic health index (MHI)" from the phenotypic measures taken from our individual mice (Figure 5A). Briefly, z-scored *in vivo* and *ex vivo* measurements were scaled by different weights then added together to create a metric to rank each animal based on their metabolic characteristics. Applying the MHI to our 26 individual mice placed the diabetic *db/db* mouse at the lowest end of the scale (Figure 5B, Data S1; Table S6). Importantly, mice did not group solely by strain, indicating that differences in the individual metabolic health of mice between strains could still be identified. Ultimately, MHI enabled correlation of individual mouse phenotypic measures with their islet proteomes. This approach is advantageous as it captures individual variance in phenotypic response, independently of strain and genetic background grouping. Using this approach we analyzed proteins quantified in every sample (6,715 proteins), revealing that 2,835 proteins were significantly correlated with the MHI (adj. $p < 0.05$). Of these, 428 proteins were selected with an $r = \pm 0.7$ cut-off, 203 and 225 of which positively and negatively correlated with MHI respectively (Figure 5C, full list of correlated proteins provided in Data S1; Table S7). An enrichment analysis of these significantly correlated proteins identified that the top 10 most positively enriched pathways were associated with mitochondrial function (Figure 5D, upper), while negatively enriched pathways included ER protein trafficking and proteasome assembly (Figure 5D, lower). We also matched

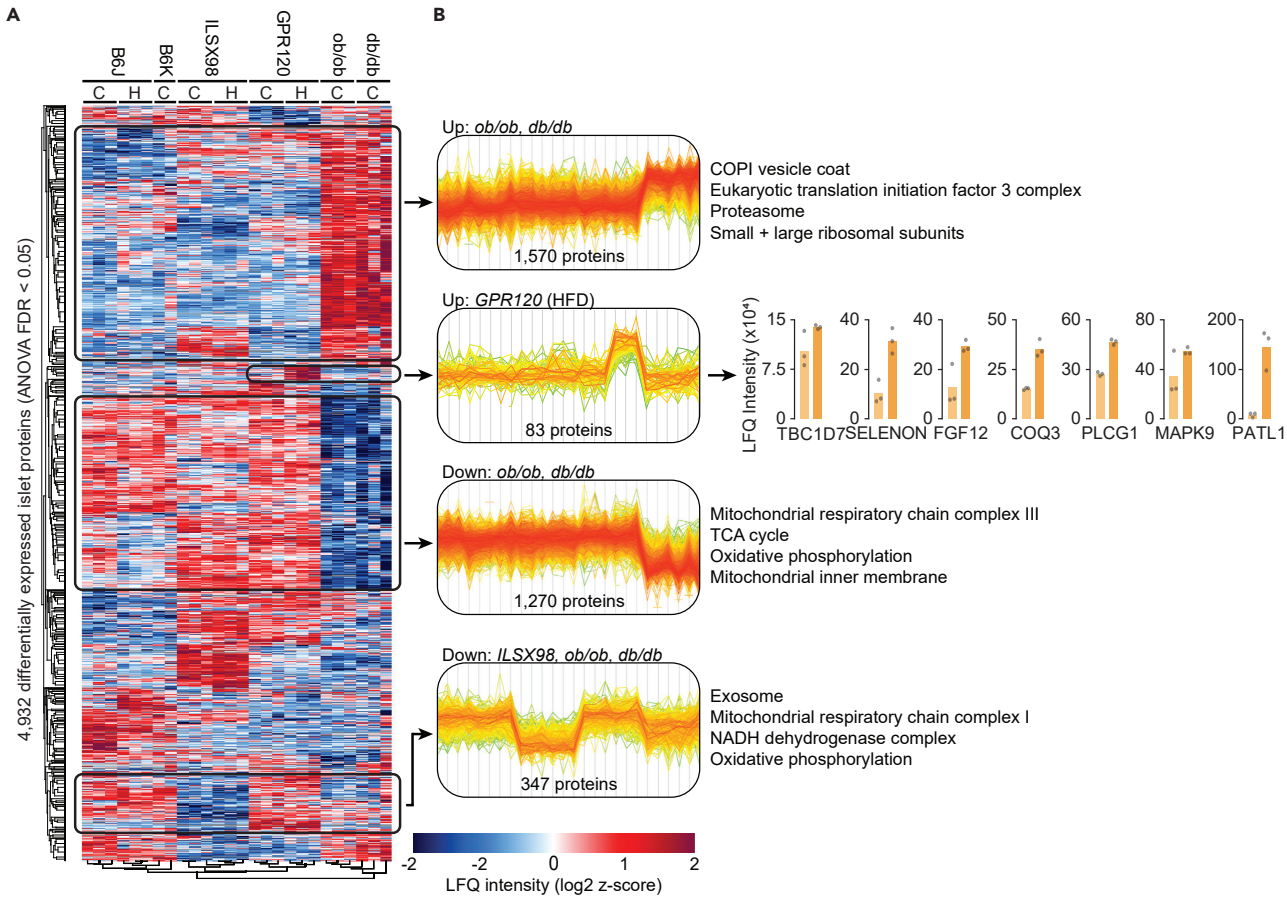

Figure 4. Unsupervised hierarchical clustering of individual mouse islet proteomes

(A) Hierarchical clustering of z-transformed log2 intensity of significantly differentially expressed proteins across all individual mouse islet proteomes.

(B) Line plots of proteins from select clusters across all individual mouse islet proteins, with enriched pathways identified in unique clusters of proteins.

our list of MHI correlated proteins to average islet protein MS intensity, generating a ranked list of islet proteins associated with metabolic health by abundance (Data S1; Table S8).

A weighted co-expression network analysis reveals key physiological islet pathways

In addition to our MHI correlation analysis, we performed a weighted gene co-expression network analysis (WGCNA) to obtain modules of highly correlated proteins within the islet proteome data sets. Here, we allowed imputation of missing proteins, to ensure both approaches were not biased by potential "specific" proteins. This yielded a total of 8,673 proteins across all islet proteomes. All proteins were assigned to one of 21 unique WGCNA modules. Modules are designated by a color name and contain 24 to 1,443 proteins. Dendrograms depict hierarchical clustering of the 21 modules (Figure S5A), as well as modules as downward branches in which the height indicates increased topological overlap between proteins (Figure S5B).

A module eigenprotein (ME), or a weighted PC1, was computed for each module. The variance in protein levels within each module that is explained by the MEs ranged from 31% to 61% (Data S1; Table S9). Figure S6A depicts the regulation of each individual islet proteome by each ME. Consistent with strain-dependent hierarchical clustering and ANOVA of total islet proteomes, strain was the primary driver of the islet proteome. MEs further stratified mouse groups, revealing interesting relationships between strains. The turquoise and blue MEs demonstrate specificity with the leptin-deficient *ob/ob* and *db/db* mouse strains, albeit in opposite directions, while the light cyan ME appears driven primarily by the B6 mouse strains (Figure S6A).

To better understand how the co-expression protein modules relate to whole-body metabolic phenotypes and *in vitro* islet function within the mice used for the islet proteomics, we computed the correlation

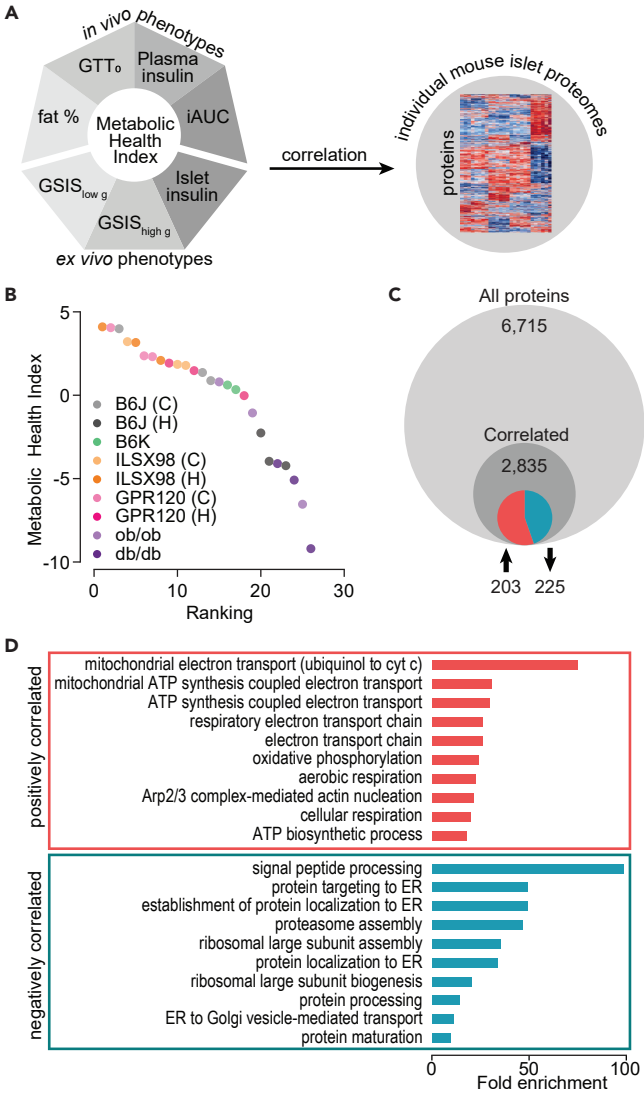

Figure 5. Establishing a Metabolic Health Index

(A) Weighted Z-scored contributions of *in vivo* and *ex vivo* phenotypes used to establish a Metabolic Health Index (MHI).

(B) Ranking of individual mice by the Metabolic Health Index identifies strain-independent unique standings.

(C) Correlation of individual mouse proteomes with MHI. Red and teal pie chart represent 203 significant positively and 225 negatively correlated proteins with $|r| > 0.7$.

(D) Top 10 identified significantly represented pathways from Gene Ontology analysis, of all significantly positively and negatively correlated proteins with MHI from (C).

between the MEs and all physiological phenotypes, as well as the previously generated MHI (Figure S6B). Among the 21 modules, 18 showed significant correlation to at least one physiological phenotype. As an example, the light yellow module negatively correlated with plasma insulin ($r = -0.44$), percentage fat mass ($r = -0.41$) and glucose at 120 min during the GTT ($r = -0.47$). Considering these negative correlations, light yellow was unsurprisingly positively correlated with MHI ($r = 0.51$). These results demonstrate that strain and diet-dependent differences in the islet proteome can yield protein modules that are strongly correlated to one or more physiological traits, where particular value lies in modules that correlated with both *in vivo* phenotypic traits and *ex vivo* islet traits. Correlation values for all MEs and physiological traits are listed in Data S1; Table S10.

Next, we performed a gene set enrichment analysis to determine which modules contain proteins overrepresenting specific physiological pathways. Each module was significantly enriched with one or more GO

or KEGG terms. The top enriched pathways ranked by *Z* score are shown in Figure S6B. Notably, the light yellow module showed the greatest enrichment overall with terms associated with mitochondria, including *mitochondrial respiratory chain complex I* (Z = 21.94), *mitochondrial respirasome* (Z = 17.4) and *NADH dehydrogenase complex* (Z = 21.94). The light yellow ME reveals that proteins within this module were relatively lower in the ILSxISS98 mice regardless of diet, and the two leptin-signaling deficient mouse modules (*ob/ob* and *db/db*), while higher in the GPR120KO, C57BL/6J and C57BL/6K mice (Figure S6A).

Identifying mitochondrial protein abundance patterns in the islet proteome

As both MHI correlation analysis and WGCNA identified mitochondrial function as a significantly represented pathway in our islet proteomes, we next examined selected mitochondrial proteins from our proteome data set. Mitocarta 3.0, a curated inventory of mitochondrial proteins (Rath et al., 2021), details sub-mitochondrial protein localization and distribution of 1,158 human and mouse genes. Although pancreas is not a tissue specifically represented by the database, Mitocarta 3.0 still provided a valuable resource that we could map to our islet proteomes and examine the expression patterns of proteins attributed to individual mitochondrial complexes (Figure S6C). Complex I proteins followed an expectedly similar expression pattern to the light yellow module (which was primarily driven by complex I protein expression), while expression patterns of complexes II, III, IV, and V displayed more subtle variations, particularly in respect to the ILSxISS98 strain (Figure S6C). Complex II proteins exhibited reduced expression in HFHSD compared to their CHOW counterparts in C57BL/6J and GPR120 KO mice, while overall and with few exceptions, both *ob/ob* and *db/db* mouse strains had significantly lower expression of numerous mitochondrial complex proteins compared to other strains.

We also investigated expression patterns of TCA cycle and TCA cycle-associated proteins, as well as proteins associated with pyruvate metabolism and calcium homeostasis in the islet proteomes (Figure S7). Lower expression of all mitochondrial metabolism-associated proteins was observed in *ob/ob* and *db/db* with only few exceptions, such as relatively high expression of the NAD-dependent malic enzymes Me2 and Me3, as well as pyruvate dehydrogenase kinase isozyme 1 (Pdk1). Interestingly, pyruvate dehydrogenase-phosphatase 1 (Pdp1) saw divergent expression in *ob/ob* and *db/db* mice, suggesting dysregulation of this enzyme may be associated with diabetes susceptibility. Additionally, glycolytic pathway proteins were also manually curated to obtain their expression patterns across the strains and diets (Figure S7). Notably, while decreased abundance of almost all glycolysis pathway proteins was observed in both *ob/ob* and non-diabetic (ND) *db/db* mice, upregulation of glucose-6-phosphate isomerase (Gpi), triosephosphate isomerase (Tpi1), enolase 1 (Eno1) and pyruvate kinase (Pklr) in the sole diabetic *db/db* (DB) mouse may indicate divergent regulation of these proteins, potentially as a consequence of its hyperglycaemia.

Interrogating islet mitochondrial function across strains

Islet mitochondrial protein expression appears to have a significant relationship with metabolic status in mice and is potentially driven by both strain and diet. To assess mitochondrial function within islets, whole islet respirometry can be used as a surrogate for mitochondrial respiration in the context of whole-cell functionality. For *ob/ob* and *db/db* mouse islets, littermate control mice were assessed on the same plate, alongside a C57BL/6J control mouse to which all plates were normalized. C57BL/6J *ob/ob* littermate controls and C57B/L/6K *db/db* littermate control islets demonstrated comparable oxygen consumption in all conditions (Figure 6A). Elevated basal respiration was observed in *ob/ob* islets compared to littermate controls (181.3 $\pm$ 24.22 pmol/min, compared with 43.6 $\pm$ 5.3 pmol/min in littermate controls, $p < 0.01$), corresponding to an increased response to oligomycin treatment (112.2 $\pm$ 14.8 pmol/min vs. 28.6 $\pm$ 9.1 pmol/min in littermate controls, $p < 0.01$). "Uncoupled" respiration, as measured by the remaining islet mitochondrial respiratory capacity after oligomycin treatment was also significantly elevated in *ob/ob* mice compared to their littermate controls (72.5 $\pm$ 16.0 pmol/min vs. 15.1 $\pm$ 8.1 pmol/min, $p < 0.05$) (Figure 6B). In contrast, *db/db* islet basal respiration was not significantly different to littermate control islets (140.4 $\pm$ 27.73 pmol/min vs. 63.1 $\pm$ 17.18 pmol/min respectively), and no significant difference in OCR at 20 mM glucose stimulation – or any other treatment – was measured (Figure 6B). The only difference between *ob/ob* and *db/db* islet respiration was observed under acute 20 mM glucose treatment ($p < 0.05$), with OCR of stimulated *ob/ob* at 211.9 $\pm$ 52.1 pmol/min, compared with 75.5 $\pm$ 5.29 pmol/min in *db/db* mice ($p < 0.05$, Figure 6B).

Finally, to determine the effects of glucose-driven metabolic stress in *ex vivo* C57BL/6J, ILSxISS98, and GPR120KO islets, islets were cultured for 48 h at 11 mM or 20 mM glucose (chronic hyperglycaemia) prior

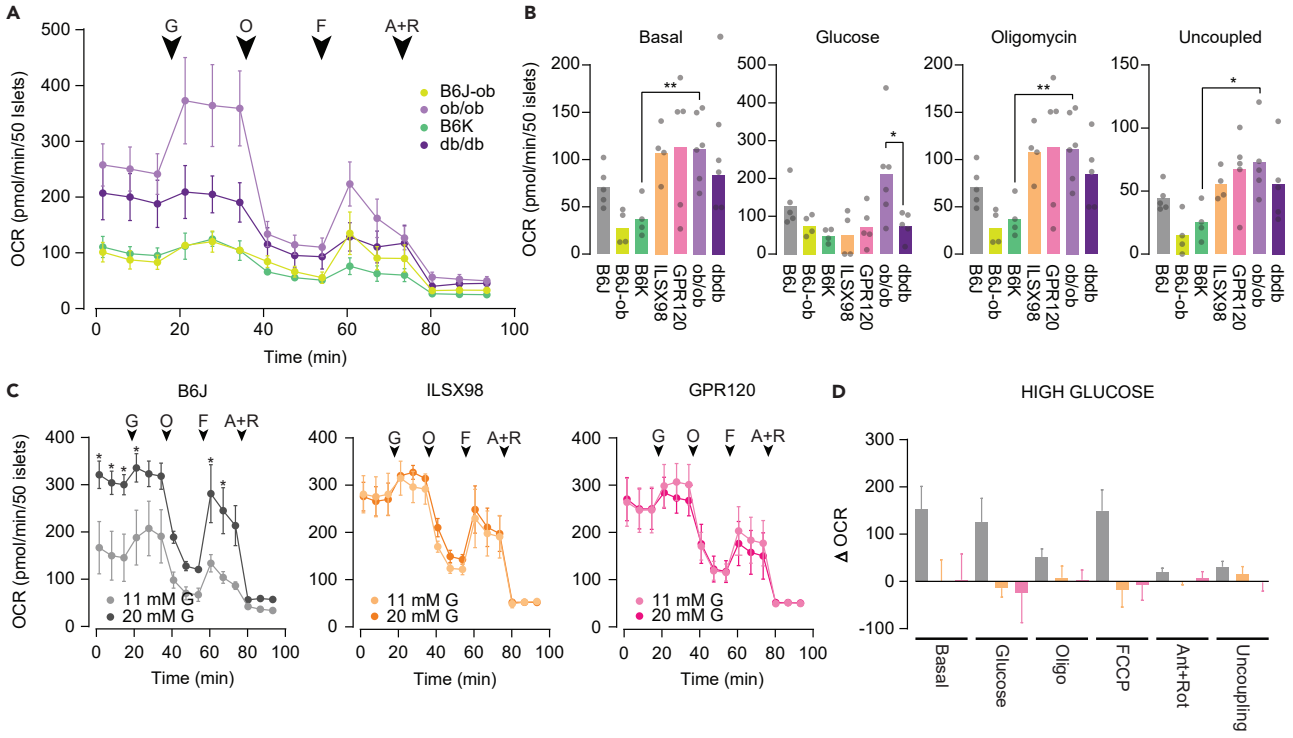

Figure 6. Islet respirometry and mitochondrial stress testing of mouse strain panel

(A) Islet respiration, measured as oxygen consumption rate (OCR), in islets from *ob/ob* and *db/db* mice, and respective C57Bl/6J and C57Bl/6K littermate controls. After 1 h basal at 2.8 mM glucose with no CO2, islets were stimulated with 20 mM glucose, oligomycin, FCCP and antimycin and rotenone at indicated timepoints.

(B) Islet respiration, measured as OCR, of all CHOW-fed strains at basal or post-stimulation with glucose or oligomycin. Uncoupled respiration measured as OCR after oligomycin stimulation less OCR after antimycin and rotenone stimulation.

(C) Islet respiration, measured as OCR, in islets from C57Bl/6J, ILSxISS98 and GPR120 KO mice after 48 h *ex vivo* culture at 11 mM or 20 mM glucose RPMI. After 1 h basal at 2.8 mM glucose with no CO2, islets were stimulated with 20 mM glucose, oligomycin, FCCP and antimycin and rotenone at indicated timepoints.

(D) Change in OCR at basal, and post-stimulations, between 11 mM and 20 mM glucose-cultured islets from C57Bl/6J, ILSxISS98 and GPR120 KO islets. *$p < 0.05$, **$p < 0.01$ using one-way ANOVA with Sidak's multiple-comparison post-test in comparisons between strains with all islet groups n = 3, data is presented as mean ± SEM.

to basal and glucose-stimulated islet respirometry measurements. Interestingly, only C57BL/6J mice exhibited changes in respiration following metabolic stress (Figure 6B), with significant increases in basal respiration (145.5 ± 50.06 pmol/min vs. 300.0 ± 21.6 pmol/min, $p < 0.05$), glucose-stimulated respiration (208.6 ± 57.7 pmol/min vs. 335.7 ± 30.2 pmol/min, $p < 0.05$), FCCP treatment (133.7 ± 18.6 pmol/min vs. 285.1 ± 135.9 pmol/min, $p < 0.05$), and "uncoupled" respiration (32.9 ± 13.4 pmol/min vs. 66.1 ± 4.7 pmol/min, $p < 0.05$), while ILSxISS98 and GPR120 KO islets did not significantly alter their respirometry profiles (Figures 6C and 6D).

DISCUSSION

Islet dysfunction, primarily characterized by β-cell failure, is a hallmark of T2D. However, the underlying factors that control the transition from healthy islet status, to islet compensation and finally to β-cell failure, are not fully understood. Our study interrogated a spectrum of islet proteomes in different mouse strains known to exhibit large variations in metabolic phenotypes. By generating a deep strain-specific library of islet proteins, our single-run measurements of individual mouse islets produced very high coverage of the islet proteome. Our islet proteomes span two diets, as well as multiple genetic backgrounds. Because we performed detailed metabolic profiling of each individual mouse using both *in vivo* and *ex vivo* measures, we were able to establish a MHI, summarizing these phenotypic outcomes. Individual mice could then be ranked, and proteins contributing most to these phenotypes identified in an unbiased manner using multiple approaches.

Our analysis revealed a strong link between metabolic health and mitochondrial function, as enriched pathways represented by the 203 significantly positively correlated proteins were primarily associated with the mitochondria. Of the significantly negatively correlated proteins, protein trafficking to the ER was also highly represented, suggesting a similarly important role for this organelle in islet health. This is concordant with previous gene expression analyses in the metabolically stressed *ob/ob* and *db/db* strains, in which upregulation of ER stress proteins was characteristic of both strains, while an increase in the unfolded protein response was only observed in islet compensation (*ob/ob*), and not diabetes (*db/db*) (Chan et al., 2013). WGCNA generated 21 modules, many of which offer valuable avenues for further exploration, including the light yellow mitochondria-associated module for its highest pathway enrichment score, and significant correlations with multiple *in vivo* traits. Notably, WGCNA has previously been used to investigate islet proteome expression networks in the 8 founder strains of the Collaborative Cross (Mitok et al., 2018), from which 25% of identified modules in those proteomes also saw enrichment for some aspect of mitochondrial function. Also in agreement with observations in our *ob/ob* and *db/db* islet data, Mitok and colleagues further reported that downregulation of mitochondrial proteins were observed in the obesity and diabetes-susceptible NZO strain, while similarly demonstrating impaired glucose-stimulated insulin secretion (Mitok et al., 2018).

The importance of mitochondrial metabolism to overall islet function is well-studied. Mitochondria are central to metabolism-secretion coupling. Glucose-sensing, uptake, and glycolysis by the β-cells of the islet feed directly into pyruvate oxidation, the TCA cycle, and oxidative phosphorylation, driving ATP synthesis and the closure of K^{+}_{ATP} channels. The resulting calcium influx triggers exocytosis of insulin granules. Mitochondrial metabolism also generates additional coupling factors that contribute to the amplifying pathway of glucose-stimulated insulin secretion (Maechler, 2013). Mitochondrial inhibition in the pancreatic islet directly affects glucose-stimulated insulin secretion (MacDonald and Fahien, 1990; Silva et al., 2000) and a mutation in mitochondrial protein has been associated with reduced insulin secretion and increased future risk of T2D (Koeck et al., 2011).

Recently, dysregulated mitochondrial metabolism has been implicated in diabetic mice (Haythorne et al., 2019). βV59M inducible-transgenic mice possess constitutively open ATP-sensitive potassium channels, resulting in an inability for the β-cells to depolarize and hence secrete insulin. These mice reflect a sudden and sustained hyperglycemic/hypoinsulinaemic phenotype with an observed upregulation of glycolytic enzymes, but downregulation in mitochondrial proteins – a pattern partially reflected in our diabetic *db/db* mouse data (Figure S7). Similarly, insulin-resistant diabetic strain MKR mouse islets were also characterized by reduced expression of TCA cycle and electron transport chain proteins (Lu et al., 2010). Interestingly, oxygen consumption was also significantly reduced in βV59M mice, primarily attributed to reduced glucose oxidation in chronic hyperglycaemia, although we found this impairment in *db/db* only apparent at 20 mM glucose stimulation (Figure 6B).

In the context of mitochondrial complex I, it is interesting to acknowledge the differences between the *ob/ob* mouse and the HFHSD-fed C57Bl/6J, as both exhibit obesity and insulin resistance on the same genetic background. Complex I protein expression did not change markedly in HFHSD-fed C57Bl/6J islets, compared to downregulation in *ob/ob* islets, however Complex II, III and IV proteins did. Both groups also exhibited downregulation of TCA cycle proteins and pyruvate metabolism compared to C57Bl/6J control mice. Additionally, ILSxISS98 mice, which were generally resistant to the effects of HFHSD and whose islets saw no significant changes in OCR after chronic hyperglycemic culture, also displayed relatively low levels of complex I protein expression in CHOW and HFHSD groups. This apparent dichotomy warrants further investigation, with complex I the largest enzyme in the mitochondrial respiratory chain and the first to encounter glycolysis substrates. Complex I dysfunction in tissues is the most common in oxidative phosphorylation disorders in humans (Ghezzi and Zeviani, 2018) and in islets is susceptible to maladaptation, with reduced complex I expression in islets with deficits in mitochondrial autophagy correlating with reduced respiration (Kim et al., 2015). Complex I is also the major contributor to NAD^{+} recycling and complex I hyperactivity, defined as an NADH/NAD^{+} redox imbalance due to increased NADH as a result of hyperglycaemia, occurs in T2D and diverts excess electrons to reactive oxygen species (ROS) production via the polyol pathway (Rolo and Palmeira, 2006; Wu et al., 2017). Indeed, elevated NADH was measured in diabetic βV59M islets at basal (Haythorne et al., 2019), while *db/db* pancreas (not islets) displayed increased complex I activity compared to control islets, as did INS-1 β-cells cultured at 20 mM glucose (Wu et al., 2017). This occurs despite unchanged complex V activity and decreased ATP output, suggesting increased mitochondrial uncoupling.

Together these data suggest that dysregulation of islet function occurs between glucose-sensing and the mitochondria in the β-cell, with excess glucose supply driving the downregulation of glycolytic enzyme activity and subsequent pyruvate metabolism, resulting in downregulation of mitochondrial complex I (and all oxidative phosphorylation machinery). Continued substrate oversupply of complex I may drive ROS generation leading eventually to β-cell failure (Maechler et al., 1999; Robertson, 2006; Robertson et al., 2004). The exception to this was apparent in relatively high glucokinase expression in both our *ob/ob* and non-diabetic *db/db* islets. This was observed despite significant compensatory increases to islet respiration at basal, increased basal insulin secretion, and the ability to further increase respiration and increased insulin release upon glucose stimulation. In contrast, the hyperglycemic diabetic state sees upregulation of glycolysis despite continued downregulated mitochondrial activity and an inability to further compensate respiration or insulin secretion upon glucose stimulation.

In summary, this study highlights the intricacies of the relationship between the whole pancreatic islet and the metabolic status of the animal. Here we have focused on mitochondrial protein expression as an indicator of metabolic health, ultimately finding that the islet is highly capable of compensatory respiration, sometimes despite increased mitochondrial uncoupling and the dysregulation of mitochondrial proteins. However, this is just one of many potential biological processes that may be elucidated from these data. We used both correlation and WGCNA-based approaches to identify large-scale perturbations to functional pathways, rather than individual proteins, although this data now provides an online resource from which specific favored proteins can be investigated or novel gene targets such as cell surface receptors identified. We found that genetic background drives the largest variations in islet protein expression, as well as outcomes to metabolic stress. How the islet senses metabolic stress – insulin resistance or hyperinsulinaemia – and translates these signals into altering protein abundance and compensatory behaviors in the islet needs further research. Altogether this study provides a valuable and comprehensive proteomic resource for the islet biology field.

Limitations of the study

Although we have exploited the use of individual animals in our study as unique biological replicates, it must be noted that we are limited by total sample size, and sample collection at a single time point of 16 weeks age and 8 week long diet. As such, metabolic changes dependent on diet duration and animal age were not able to be investigated in this study. Additionally, we have only examined male mice in both whole-body metabolic and islet phenotyping, and there is abundant evidence for sexual dimorphism in various measurements of metabolic outcomes (Gannon et al., 2018). Islet physiology can also be confounded in single sex studies, and it is therefore necessary to acknowledge that these findings should be validated in female subjects. Specifically in respect to the *db/db* mouse strain, which is susceptible to the development of T2D, we note the limitation of mouse numbers. The *db/db* mouse undergoes various stages of metabolic dysfunction in the progression of T2D (Do et al., 2016), and in our first cohort by 16 weeks, only one mouse had developed T2D.

Finally, as the pancreatic islet consists of multiple cell types, making conclusions specifically regarding β-cell function can be erroneous. Beta-cells make up an approximate 70–80% of an islet's cellular composition (Kulkarni, 2004), but this percentage may change depending on genetic background. Using WGCNA modules, we attempted to investigate cell type-specific protein expression across strains. While the blue module was easily identified as the "β-cell module", subscribing a host of β-cell specific genes (Data S1; Table S11, Figure 5B), we also identified modules enriched with proteins specific to alpha and delta-cells using glucagon and somatostatin). Although the regulation of these proteins is informative, it must still be noted that the relative protein expression of single cell type may only be indicative of overall proportional changes to a whole islet.

STAR★METHODS

Detailed methods are provided in the online version of this paper and include the following:

- KEY RESOURCES TABLE
- RESOURCE AVAILABILITY
  - Lead contact
  - Materials availability
  - Data and code availability

SUPPLEMENTAL INFORMATION

Supplemental information can be found online at https://doi.org/10.1016/j.isci.2021.103099.

ACKNOWLEDGMENTS

We thank Professor Alan D Attie, University of Wisconsin-Madison for insightful discussions. This research was facilitated by access to Sydney Mass Spectrometry, a core research facility at the University of Sydney. We thank Ben Crossett, Angela Connolly, and Jens Altvater for technical assistance. M.A.K is supported by a Jennie Mackenzie Philanthropic Fellowship, University of Sydney. S.C. is supported by a UNSW Scientia PhD Scholarship. M.R.S., L.M.S., and A.V.C. are supported by National Cancer Institute of the National Institute of Health under award number R01CA193481. M.P.K was supported by the University of Wisconsin–Madison, Department of Biochemistry and Office of the Vice Chancellor for Research and Graduate Education with funding from the Wisconsin Alumni Research Foundation.

AUTHOR CONTRIBUTIONS

Conceptualization, S.J.H. and M.A.K.; methodology and validation, B.Y. and S.J.H.; formal analysis, B.Y., S.N., A.D., A.V.C., J.V.G., and S.J.H.; investigation; B.Y, S.N., A.D., E.N., and S.J.H.; data curation and visualization B.Y., S.N., and S.J.H.; writing – original draft, B.Y., S.N., M.P.K., and M.A.K.; writing – review & editing; B.Y., S.N., A.D., A.V.G., E.N., D.J., S.C., G.C., P.T., M.L., S.J.H., and M.A.K.; project administration; B.Y., S.N., and M.A.K.; software, M.L.; resources, D.J., S.C., K.L.H., A.E.B., L.M., G.C., P.T., D.E.J., and M.A.K.; supervision, M.R.S., L.M.S., M.P.K., D.E.J., S.J.H., and M.A.K.; funding acquisition, M.A.K. M.A.K. is a consulting editor for iScience.

DECLARATION OF INTERESTS

The authors declare no competing financial or non-financial interests.

Received: April 29, 2021
Revised: August 9, 2021
Accepted: September 6, 2021
Published: October 22, 2021

REFERENCES

Ahren, B., and Scheurink, A.J. (1998). Marked hyperleptinemia after high-fat diet associated with severe glucose intolerance in mice. Eur. J. Endocrinol. *139*, 461–467.

Alarcon, C., Boland, B.B., Uchizono, Y., Moore, P.C., Peterson, B., Rajan, S., Rhodes, O.S., Noske, A.B., Haataja, L., Arvan, P., et al. (2016). Pancreatic beta-cell adaptive plasticity in obesity increases insulin production but adversely affects secretory function. Diabetes *65*, 438–450.

American Diabetes, A. (2011). Standards of medical care in diabetes–2011. Diabetes Care *34*, S11–S61.

Antonetti, D.A., Silva, P.S., and Stitt, A.W. (2021). Current understanding of the molecular and cellular pathology of diabetic retinopathy. Nat. Rev. Endocrinol. *17*, 195–206.

Bays, H.E., Chapman, R.H., Grandy, S., and Group, S.I. (2007). The relationship of body mass index to diabetes mellitus, hypertension and dyslipidaemia: comparison of data from two national surveys. Int. J. Clin. Pract. *61*, 737–747.

Bennett, B., Carosone-Link, P., Zahniser, N.R., and Johnson, T.E. (2006). Confirmation and fine mapping of ethanol sensitivity quantitative trait loci, and candidate gene testing in the LXS recombinant inbred mice. J. Pharmacol. Exp. Ther. *319*, 299–307.

Chan, J.Y., Luzuriaga, J., Bensellam, M., Biden, T.J., and Laybutt, D.R. (2013). Failure of the adaptive unfolded protein response in islets of obese mice is linked with abnormalities in beta-cell gene expression and progression to diabetes. Diabetes *62*, 1557–1568.

Chapman, J.D., Goodlett, D.R., and Masselon, C.D. (2014). Multiplexed and data-independent tandem mass spectrometry for global proteome profiling. Mass Spectrom. Rev. *33*, 452–470.

Chen, H., Charlat, O., Tartaglia, L.A., Woolf, E.A., Weng, X., Ellis, S.J., Lakey, N.D., Culpepper, J., Moore, K.J., Breitbart, R.E., et al. (1996). Evidence that the diabetes gene encodes the leptin receptor: identification of a mutation in the leptin receptor gene in db/db mice. Cell *84*, 491–495.

Clark, A., Jones, L.C., de Koning, E., Hansen, B.C., and Matthews, D.R. (2001). Decreased insulin secretion in type 2 diabetes: a problem of cellular mass or function? Diabetes *50*, S169–S171.

Cox, J., and Mann, M. (2008). MaxQuant enables high peptide identification rates, individualized p.p.b.-range mass accuracies and proteome-wide protein quantification. Nat. Biotechnol. *26*, 1367–1372.

Croze, M.L., Flisher, M.F., Guillaume, A., Tremblay, C., Noguchi, G.M., Granziera, S., Vivot, K., Castillo, V.C., Campbell, S.A., Ghislain, J., et al. (2021). Free fatty acid receptor 4 inhibitory signaling in delta cells regulates islet hormone secretion in mice. Mol. Metab. *45*, 101166.

Do, O.H., Gunton, J.E., Gaisano, H.Y., and Thorn, P. (2016). Changes in beta cell function occur in prediabetes and early disease in the Lepr (db) mouse model of diabetes. Diabetologia *59*, 1222–1230.

Friedman, J.M., and Halaas, J.L. (1998). Leptin and the regulation of body weight in mammals. Nature *395*, 763–770.

Gannon, M., Kulkarni, R.N., Tse, H.M., and Mauvais-Jarvis, F. (2018). Sex differences underlying pancreatic islet biology and its dysfunction. Mol. Metab. *15*, 82–91.

Ghezzi, D., and Zeviani, M. (2018). Human diseases associated with defects in assembly of OXPHOS complexes. Essays Biochem. *62*, 271–286.

Gotoh, C., Hong, Y.H., Iga, T., Hishikawa, D., Suzuki, Y., Song, S.H., Choi, K.C., Adachi, T., Hirasawa, A., Tsujimoto, G., et al. (2007). The regulation of adipogenesis through GPR120. Biochem. Biophys. Res. Commun. *354*, 591–597.

Groop, L., and Lyssenko, V. (2009). Genetic basis of beta-cell dysfunction in man. Diabetes Obes. Metab. *11*, 149–158.

Halban, P.A., Polonsky, K.S., Bowden, D.W., Hawkins, M.A., Ling, C., Mather, K.J., Powers, A.C., Rhodes, C.J., Sussel, L., and Weir, G.C. (2014). beta-cell failure in type 2 diabetes: postulated mechanisms and prospects for prevention and treatment. J. Clin. Endocrinol. Metab. *99*, 1983–1992.

Harding, J.L., Pavkov, M.E., Magliano, D.J., Shaw, J.E., and Gregg, E.W. (2019). Global trends in diabetes complications: a review of current evidence. Diabetologia *62*, 3–16.

Harney, D.J., Hutchison, A.T., Hatchwell, L., Humphrey, S.J., James, D.E., Hocking, S., Heilbronn, L.K., and Larance, M. (2019). Proteomic analysis of human plasma during intermittent fasting. J. Proteome Res. *18*, 2228–2240.

Haythorne, E., Rohm, M., van de Bunt, M., Brereton, M.F., Tarasov, A.I., Blacker, T.S., Sachse, G., Silva Dos Santos, M., Terron Exposito, R., Davis, S., et al. (2019). Diabetes causes marked inhibition of mitochondrial metabolism in pancreatic beta-cells. Nat. Commun. *10*, 2474.

Hirasawa, A., Tsumaya, K., Awaji, T., Katsuma, S., Adachi, T., Yamada, M., Sugimoto, Y., Miyazaki, S., and Tsujimoto, G. (2005). Free fatty acids regulate gut incretin glucagon-like peptide-1 secretion through GPR120. Nat. Med. *11*, 90–94.

Hudish, L.I., Reusch, J.E., and Sussel, L. (2019). Beta Cell dysfunction during progression of metabolic syndrome to type 2 diabetes. J. Clin. Invest. *129*, 4001–4008.

Ichimura, A., Hirasawa, A., Poulain-Godefroy, O., Bonnefond, A., Hara, T., Yengo, L., Kimura, I., Leloire, A., Liu, N., Iida, K., et al. (2012). Dysfunction of lipid sensor GPR120 leads to obesity in both mouse and human. Nature *483*, 350–354.

Kahn, S.E. (2003). The relative contributions of insulin resistance and beta-cell dysfunction to the pathophysiology of Type 2 diabetes. Diabetologia *46*, 3–19.

Kang, T., Boland, B.B., Alarcon, C., Grimsby, J.S., Rhodes, C.J., and Larsen, M.R. (2019). Proteomic analysis of restored insulin production and trafficking in obese diabetic mouse pancreatic islets following euglycemia. J. Proteome Res. *18*, 3245–3258.

Kang, T., Boland, B.B., Jensen, P., Alarcon, C., Nawrocki, A., Grimsby, J.S., Rhodes, C.J., and Larsen, M.R. (2020). Characterization of signaling pathways associated with pancreatic beta-cell adaptive flexibility in compensation of obesity-linked diabetes in db/db mice. Mol. Cell Proteomics *19*, 971–993.

Keller, M.P., Rabaglia, M.E., Schueler, K.L., Stapleton, D.S., Gatti, D.M., Vincent, M., Mitok, K.A., Wang, Z., Ishimura, T., Simonett, S.P., et al. (2019). Gene loci associated with insulin secretion in islets from non-diabetic mice. J. Clin. Invest. *129*, 4419–4432.

Kim, M.J., Choi, O.K., Chae, K.S., Kim, M.K., Kim, J.H., Komatsu, M., Tanaka, K., Lee, H., Chung, S.S., Kwak, S.H., et al. (2015). Mitochondrial complexes I and II are more susceptible to autophagy deficiency in mouse beta-cells. Endocrinol. Metab. (Seoul) *30*, 65–70.

Koeck, T., Olsson, A.H., Nitert, M.D., Sharoyko, V.V., Ladenvall, C., Kotova, O., Reiling, E., Ronn, T., Parikh, H., Taneera, J., et al. (2011). A common variant in TFB1M is associated with reduced insulin secretion and increased future risk of type 2 diabetes. Cell Metab. *13*, 80–91.

Kulak, N.A., Pichler, G., Paron, I., Nagaraj, N., and Mann, M. (2014). Minimal, encapsulated proteomic-sample processing applied to copy-number estimation in eukaryotic cells. Nat. Methods *11*, 319–324.

Kulkarni, R.N. (2004). The islet beta-cell. Int. J. Biochem. Cell Biol. *36*, 365–371.

Langfelder, P., and Horvath, S. (2008). WGCNA: an R package for weighted correlation network analysis. BMC Bioinformatics *9*, 559.

Langfelder, P., and Horvath, S. (2012). Fast R functions for robust correlations and hierarchical clustering. J. Stat. Softw. *46*, 17.

Liao, C.Y., Rikke, B.A., Johnson, T.E., Diaz, V., and Nelson, J.F. (2010). Genetic variation in the murine lifespan response to dietary restriction: from life extension to life shortening. Aging Cell *9*, 92–95.

Liu, M., Huang, Y., Xu, X., Li, X., Alam, M., Arunagiri, A., Haataja, L., Ding, L., Wang, S., Itkin-Ansari, P., et al. (2021). Normal and defective pathways in biogenesis and maintenance of the insulin storage pool. J. Clin. Invest. *131*, e142240.

Lu, H., Koshkin, V., Allister, E.M., Gyulkhandanyan, A.V., and Wheeler, M.B. (2010). Molecular and metabolic evidence for mitochondrial defects associated with beta-cell dysfunction in a mouse model of type 2 diabetes. Diabetes *59*, 448–459.

MacDonald, M.J., and Fahien, L.A. (1990). Insulin release in pancreatic islets by a glycolytic and a Krebs cycle intermediate: contrasting patterns of glyceraldehyde phosphate and succinate. Arch. Biochem. Biophys. *279*, 104–108.

Maechler, P. (2013). Mitochondrial function and insulin secretion. Mol. Cell. Endocrinol. *379*, 12–18.

Maechler, P., Jornot, L., and Wollheim, C.B. (1999). Hydrogen peroxide alters mitochondrial activation and insulin secretion in pancreatic beta cells. J. Biol. Chem. *274*, 27905–27913.

Metz, T.O., Jacobs, J.M., Gritsenko, M.A., Fontes, G., Qian, W.J., Camp, D.G., 2nd, Poitout, V., and Smith, R.D. (2006). Characterization of the human pancreatic islet proteome by two-dimensional LC/MS/MS. J. Proteome Res. *5*, 3345–3354.

Mitok, K.A., Freiberger, E.C., Schueler, K.L., Rabaglia, M.E., Stapleton, D.S., Kwiecien, N.W., Malec, P.A., Hebert, A.S., Broman, A.T., Kennedy, R.T., et al. (2018). Islet proteomics reveals genetic variation in dopamine production resulting in altered insulin secretion. J. Biol. Chem. *293*, 5860–5877.

Moran, B.M., Abdel-Wahab, Y.H., Flatt, P.R., and McKillop, A.M. (2014). Evaluation of the insulin-releasing and glucose-lowering effects of GPR120 activation in pancreatic beta-cells. Diabetes Obes. Metab. *16*, 1128–1139.

Nakayasu, E.S., Syed, F., Tersey, S.A., Gritsenko, M.A., Mitchell, H.D., Chan, C.Y., Dirice, E., Turatsinze, J.V., Cui, Y., Kulkarni, R.N., et al. (2020). Comprehensive proteomics analysis of stressed human islets identifies GDF15 as a target

for type 1 diabetes intervention. Cell Metab. *31*, 363–374 e366.

Newton, M.A., Quintana, F.A., Den Boon, J.A., Sengupta, S., and Ahlquist, P. (2007). Random-set methods identify distinct aspects of the enrichment signal in gene-set analysis. Ann. Appl. Stat. *1*, 85–106.

Oh, D.Y., Talukdar, S., Bae, E.J., Imamura, T., Morinaga, H., Fan, W., Li, P., Lu, W.J., Watkins, S.M., and Olefsky, J.M. (2010). GPR120 is an omega-3 fatty acid receptor mediating potent anti-inflammatory and insulin-sensitizing effects. Cell *142*, 687–698.

Petyuk, V.A., Qian, W.J., Hinault, C., Gritsenko, M.A., Singhal, M., Monroe, M.E., Camp, D.G., 2nd, Kulkarni, R.N., and Smith, R.D. (2008). Characterization of the mouse pancreatic islet proteome and comparative analysis with other mouse tissues. J. Proteome Res. *7*, 3114–3126.

Rath, S., Sharma, R., Gupta, R., Ast, T., Chan, C., Durham, T.J., Goodman, R.P., Grabarek, Z., Haas, M.E., Hung, W.H.W., et al. (2021). MitoCarta3.0: an updated mitochondrial proteome now with sub-organelle localization and pathway annotations. Nucleic Acids Res. *49*, D1541–D1547.

Robertson, R.P. (2006). Oxidative stress and impaired insulin secretion in type 2 diabetes. Curr. Opin. Pharmacol. *6*, 615–619.

Robertson, R.P., Harmon, J., Tran, P.O., and Poitout, V. (2004). Beta-cell glucose toxicity, lipotoxicity, and chronic oxidative stress in type 2 diabetes. Diabetes *53*, S119–S124.

Rolo, A.P., and Palmeira, C.M. (2006). Diabetes and mitochondrial function: role of hyperglycemia and oxidative stress. Toxicol. Appl. Pharmacol. *212*, 167–178.

Schrimpe-Rutledge, A.C., Fontes, G., Gritsenko, M.A., Norbeck, A.D., Anderson, D.J., Waters, K.M., Adkins, J.N., Smith, R.D., Poitout, V., and Metz, T.O. (2012). Discovery of novel glucose-regulated proteins in isolated human pancreatic islets using LC-MS/MS-based proteomics. J. Proteome Res. *11*, 3520–3532.

Schwanhausser, B., Busse, D., Li, N., Dittmar, G., Schuchhardt, J., Wolf, J., Chen, W., and Selbach, M. (2011). Global quantification of mammalian gene expression control. Nature *473*, 337–342.

Shields, B.M., Peters, J.L., Cooper, C., Powell, R.J., Knight, B.A., Hyde, C., and Hattersley, A.T. (2012). Identifying clinical criteria to predict Type 1 diabetes, as defined by absolute insulin deficiency: a systematic review protocol. BMJ Open *2*, e002309.

Silva, J.P., Kohler, M., Graff, C., Oldfors, A., Magnuson, M.A., Berggren, P.O., and Larsson, N.G. (2000). Impaired insulin secretion and beta-cell loss in tissue-specific knockout mice with mitochondrial diabetes. Nat. Genet. *26*, 336–340.

Stockli, J., Fisher-Wellman, K.H., Chaudhuri, R., Zeng, X.Y., Fazakerley, D.J., Meoli, C.C., Thomas, K.C., Hoffman, N.J., Mangiafico, S.P., Xirouchaki, C.E., et al. (2017). Metabolomic analysis of insulin resistance across different mouse strains and diets. J. Biol. Chem. *292*, 19135–19145.

Stone, V.M., Dhayal, S., Brocklehurst, K.J., Lenaghan, C., Sorhede Winzell, M., Hammar, M., Xu, X., Smith, D.M., and Morgan, N.G. (2014). GPR120 (FFAR4) is preferentially expressed in pancreatic delta cells and regulates somatostatin secretion from murine islets of Langerhans. Diabetologia *57*, 1182–1191.

Stumvoll, M., Fritsche, A., and Haring, H.U. (2002). Clinical characterization of insulin secretion as the basis for genetic analyses. Diabetes *51*, S122–S129.

Suckow, A.T., Polidori, D., Yan, W., Chon, S., Ma, J.Y., Leonard, J., and Briscoe, C.P. (2014). Alteration of the glucagon axis in GPR120 (FFAR4) knockout mice: a role for GPR120 in glucagon secretion. J. Biol. Chem. *289*, 15751–15763.

Surwit, R.S., Kuhn, C.M., Cochrane, C., McCubbin, J.A., and Feinglos, M.N. (1988). Diet-induced type II diabetes in C57BL/6J mice. Diabetes *37*, 1163–1167.

Taddeo, E.P., Stiles, L., Sereda, S., Ritou, E., Wolf, D.M., Abdullah, M., Swanson, Z., Wilhelm, J., Bellin, M., McDonald, P., et al. (2018). Individual islet respirometry reveals functional diversity within the islet population of mice and human donors. Mol. Metab. *16*, 150–159.

Tanaka, T., Katsuma, S., Adachi, T., Koshimizu, T.A., Hirasawa, A., and Tsujimoto, G. (2008). Free fatty acids induce cholecystokinin secretion through GPR120. Naunyn Schmiedebergs Arch. Pharmacol. *377*, 523–527.

Thomas, D.D., Corkey, B.E., Istfan, N.W., and Apovian, C.M. (2019). Hyperinsulinemia: an early indicator of metabolic dysfunction. J. Endocr. Soc. *3*, 1727–1747.

Tyanova, S., Temu, T., Sinitcyn, P., Carlson, A., Hein, M.Y., Geiger, T., Mann, M., and Cox, J. (2016). The Perseus computational platform for comprehensive analysis of (prote)omics data. Nat. Methods *13*, 731–740.

Udeshi, N.D., Svinkina, T., Mertins, P., Kuhn, E., Mani, D.R., Qiao, J.W., and Carr, S.A. (2013). Refined preparation and use of anti-diglycine remnant (K-epsilon-GG) antibody enables routine quantification of 10,000s of ubiquitination sites in single proteomics experiments. Mol. Cell. Proteomics *12*, 825–831.

Villafuerte, B.C., Barati, M.T., Rane, M.J., Isaacs, S., Li, M., Wilkey, D.W., and Merchant, M.L. (2017). Over-expression of insulin-response element binding protein-1 (IRE-BP1) in mouse pancreatic islets increases expression of RACK1 and TCTP: beta cell markers of high glucose sensitivity. Biochim. Biophys. Acta Proteins Proteom. *1865*, 186–194.

Williams, R.W., Bennett, B., Lu, L., Gu, J., DeFries, J.C., Carosone-Link, P.J., Rikke, B.A., Belknap, J.K., and Johnson, T.E. (2004). Genetic structure of the LXS panel of recombinant inbred mouse strains: a powerful resource for complex trait analysis. Mamm. Genome *15*, 637–647.

Wortham, M., Benthuysen, J.R., Wallace, M., Savas, J.N., Mulas, F., Divakaruni, A.S., Liu, F., Albert, V., Taylor, B.L., Sui, Y., et al. (2018). Integrated in vivo quantitative proteomics and nutrient tracing reveals age-related metabolic rewiring of pancreatic beta cell function. Cell Rep. *25*, 2904–2918.e8.

Wu, J., Luo, X., Thangthaeng, N., Sumien, N., Chen, Z., Rutledge, M.A., Jing, S., Forster, M.J., and Yan, L.J. (2017). Pancreatic mitochondrial complex I exhibits aberrant hyperactivity in diabetes. Biochem. Biophys. Rep. *11*, 119–129.

Yau, B., Hays, L., Liang, C., Laybutt, D.R., Thomas, H.E., Gunton, J.E., Williams, L., Hawthorne, W.J., Thorn, P., Rhodes, C.J., et al. (2020). A fluorescent timer reporter enables sorting of insulin secretory granules by age. J. Biol. Chem. *295*, 8901–8911.

Zhang, L., Lanzoni, G., Battarra, M., Inverardi, L., and Zhang, Q. (2017). Proteomic profiling of human islets collected from frozen pancreata using laser capture microdissection. J. Proteomics *150*, 149–159.

STAR★METHODS

KEY RESOURCES TABLE

REAGENT or RESOURCE	SOURCE	IDENTIFIER
Chemicals, peptides, and recombinant proteins		
Liberase TM Research Grade	Thermo Fisher	#5401119001
Histopaque 1077	Sigma-Aldrich	#10771
Histopaque 1119	Sigma Aldrich	#11191
HBSS	Thermo Fisher	#14185052
Bovine Serum Albumin (BSA) ≥96%, Fatty acid free	Sigma-Aldrich	#A6003
Glucose 50%	Vital Medical Supplies	#AS3017
RPMI 1640 Medium	Thermo Fisher	#11875119
Fetal Bovine Serum, AU origin	Merck	#12003C
Penicillin/Streptomycin	Thermo Fisher	#15140122
HEPES >99.5% titration	Sigma	#H3375
Sodium orthovanadate	Sigma	#S6508
Tris(2-carboxyethyl)phosphine hydrochloride TCEP	Thermo Fisher	#PG82089
2-Chloroacetamide (CAA)	Sigma-Aldrich	#22790
Trypsin	Sigma-Aldrich	
LysC	Wako	
sodium deoxycholate	Sigma	#D6750
1% trifluoroacetic acid (TFA)	Merck	
Ethyl acetate (for HPLC)	Fisher Scientific	#E090617
Acetonitrile (ACN) (Optima LC/MS Grade)	Fisher Scientific	#A9554
Critical commercial assays		
Seahorse XF Cell Mito Stress Test Kit	Agilent	#103015-100
Pierce BCA Protein Assay	Pierce	#23225
Ultra-Sensitive Mouse Insulin ELISA kit	Crystal Chem	#90080
Quant-iT PicoGreen dsDNA Assay kit	Thermo Fisher	#P7589
Deposited data		
Raw and analyzed data	This paper	PRIDE proteomeXchange; accession PXD024522
Experimental models: Organisms/strains		
C57Bl/6J	Australian BioResources	https://www.abr.org.au/
C57Bl/6K	The Jackson Laboratory	www.jax.org
BKS.Cg- Leprob/J (*ob/ob*)	Australian BioResources	https://www.abr.org.au/
GPR120 KO	Australian Phenotype Network	Knockout mouse project (KOMP project ID VG15078)
BKS.Cg-Dock7m+/+Leprdb/J (*db/db*)	The Jackson Laboratory	www.jax.org
ILSxISS98	The Jackson Laboratory	www.jax.org
Software and algorithms		
GraphPad Prism 8.0	GraphPad	www.graphpad.com
Perseus	Max Quant	www.maxquant.net/perseus/
R studio	RStudio	www.rstudio.com

(*Continued on next page*)

Continued

REAGENT or RESOURCE	SOURCE	IDENTIFIER
R	R software	www.r-project.org
MetaNetwork	R package	https://github.com/smith-chem-wisc/MetaNetwork
Gene Ontology Enrichment	R application	https://github.com/lengning/Enrich_shiny

RESOURCE AVAILABILITY

Lead contact

Further information and requests for resources should be directed to the lead contact Melkam A Kebede (melkam.kebede@sydney.edu.au), University of Sydney, Camperdown, Australia.

Materials availability

This study did not generate new reagents.

Data and code availability

- All raw and processed proteomics data are available in the PRIDE proteomeXchange (https://www.ebi.ac.uk/pride/) repository, with the accession PXD024522 reviewer_pxd024522@ebi.ac.uk. Further processed data are available as supplementary tables in Data S1. Proteome data may also be searched online at https://kebedelab.com/islet-proteome-resource.
- This paper does not report original code.
- Any additional information required to reanalyze the data reported in this paper is available from the lead contact upon request.

EXPERIMENTAL MODEL AND SUBJECT DETAILS

Animals

All mouse subjects used in this study were male. Mice were fed ad libitum a standard laboratory chow (8% of calories from fat) or a HFHSD (48% fat [7:1 lard-to-safflower oil ratio], 32% carbohydrate, 20% protein) for 8-weeks. Diet intervention began at 8 weeks of age, was provided ad libitum, and mice were weighed weekly. *In vivo* phenotyping was performed at 14 – 15 weeks age, and euthanasia for *ex vivo* phenotyping at 15 – 16 weeks age.

All strains were backcrossed at least 10 generations to their respective genetic background at time of study. C57BL/6J mice were purchased from Australian BioResources (Moss Vale, New South Wales, Australia). The GPR120 KO mice were purchased from the Australian Phenotype Network and generated by Knockout mouse project (KOMP project ID VG15078). BKS.Cg- Leprob/J (ob/ob) mice were obtained from Garvan Institute breeding colonies (Australian BioResources, Moss Vale, New South Wales, Australia). BKS.Cg-Dock7m+/+Leprdb/J (db/db) mice were bred at the Charles Perkins Centre, University of Sydney, Australia. The ILSxISS98 strain was purchased from Jackson Laboratories, USA. All mice were transferred to at least 2 weeks prior to experimental procedures for acclimatisation and housed with food provided ad libitum on a standard light/dark cycle within the at the Laboratory Animal Services BSU Facility at the Charles Perkins Centre, University of Sydney, Australia, which routinely tests health status.

All procedures performed followed the National Health and Medical Research Council guidelines for animal research and were approved by the University of Sydney Animal Ethics Committee.

METHOD DETAILS

Intraperitoneal glucose tolerance test (IP-GTT)

Mice were fasted for 6 hours prior to IP-GTT. Magnetic resonance imaging (MRI) was conducted (EchoMRI 900) to determine lean and fat mass and mice were intraperitoneally injected with glucose (2 g / kg lean mass). Blood glucose was measured immediately prior to and 15, 30, 45, 60 and 90 min after glucose injection with ACCU-CHEK Performa II (Roche, Basel, CH). Blood was collected immediately prior to and

15 minutes after glucose injection and plasma insulin measured using the Ultra-Sensitive Mouse Insulin ELISA kit (Crystal Chem, ELK Grove Village, IL, US).

Islet isolation

At 15 - 16 weeks age, mice were euthanized by cervical dislocation, and islets were isolated (Yau et al., 2020). Briefly, the ampulla at the duodenum wall is clamped and the pancreata were perfused with 2 mL of 0.25 mg / mL liberase (Roche, Basel, CH) via injection of the common bile duct. Pancreata were excised and digested for 13 minutes at 37°C then washed in HBSS buffer (Gibco, Carlsbad, CA, US), centrifugating at 500 x g for 3 min. The pellet was resuspended, filtered through a mesh to remove any undigested tissue and centrifuged again (500 x g, 3 min). The resulting pellet was resuspended in a Histopaque 1119 and 1077 gradient (Sigma-Aldrich, St. Louis, MO, US), and spun at 1000 x g, 20 min, no brake. Islets were washed once in HBSS (700 x g, 3 min), handpicked under a stereomicroscope and recovered in Islet Media (RPMI, 10% FBS, 1% penicillin/streptomycin).

Glucose-stimulated insulin secretion (GSIS)

Islets were incubated in 2.8 mM glucose Krebs Ringer buffer supplemented with 10 mM HEPES (KRBH) for 1 hour at 37°C, 5% CO2 before stimulation at either 2.8 mM or 16.7 mM glucose in KRBH for 1 hour, at 37°C, 5% CO2. Supernatant was collected and assayed for insulin with ELISA (Crystal Chem, USA). Islet pellets were lysed with Islet Lysis Buffer (100 mM Tris, 300 mM NaCl, 10 mM NaF, 2 mM sodium orthovanadate) and measured for total DNA and insulin content by PicoGreen dsDNA Assay kit (Thermo Fisher) and Insulin ELISA respectively. Insulin secretion measurements were normalized per 5 islets used in each condition. Total insulin content measurements were normalized to total islet DNA content.

Islet cell sample preparation (in-StageTip processing)

Sample preparation of isolated islets was performed using the in-StageTip protocol (Kulak et al., 2014). Briefly, islet cells were lysed with SDC lysis buffer (1% sodium deoxycholate/100 mM Tris pH 8.5) with boiling at 95°C for 5 minutes, followed by sonication (QSonica-Q800, 4°C 10 minutes, 95% power). Protein was quantified by BCA assay, and 40 μg protein reduced and alkylated by the addition of 10 mM TCEP (Tris(2-carboxyethyl)phosphine hydrochloride) and 40 mM CAA (2-Chloroacetamide) for 5 mins at 45°C. Protein was digested in 50 μL by the addition of trypsin (Sigma-Aldrich) and LysC (Wako) at a ratio of 1:50 for 16 h at 37°C. After digestion, peptides were diluted 50% by the addition of water, followed by the addition of 100 μL ethyl acetate/1% trifluoroacetic acid (TFA) with vigorous mixing (2 min, 2,000 rpm). Peptides were de-salted using six-layer SDBRPS StageTips, using an in-house 3D printed device to facilitate parallel sample processing (Harney et al., 2019). Bound peptides were washed with 100 μL 1% TFA in ethyl acetate, then 100 μL 1% TFA in isopropanol and finally with 0.2% TFA in 5% ACN. Desalted peptides were eluted from the StageTips with 60 μL 60%0 ACN/0.5% NH_4OH into PCR-strip tubes and dried in a vacuum concentrator prior to resuspension in 20 μL MS buffer (2% ACN/0.3% TFA).

Offline high-pH reversed-phase peptide fractionation

A deep tissue-specific islet library was created using islet peptides pooled from 3 - 6 biological replicates of each strain to generate 6 different islet samples representing all strains studied. These islet peptides were subsequently fractionated with high pH reverse phase fractionation as described (Udeshi et al., 2013) with minor modifications. Fractionation was performed using an UltiMate 3000 HPLC (Dionex, Thermo) using a XBridge Peptide BEH C18 column, (130Å, 3.5 μm 2.1 × 250 mm, Waters). 18 μg of peptides were resuspended in buffer A and loaded onto the column maintained at 50°C. Buffer A comprised 10 mM ammonium formate/2% ACN and buffer B 10 mM ammonium formate/80% ACN. Both buffers were adjusted to pH 9.0 with ammonium hydroxide. Peptides were separated by a gradient of 10 - 40% buffer B over 4.4 min, followed by 40 - 100% buffer B over 1 min. Peptides were collected for a total duration of 6.4 min, with 48 fractions concatenated directly into 16 wells of a 96-well deep-well plate (3 concatenated fractions per well) with an automated fraction collector (Dionex, Thermo) maintained at 4°C. After fraction collection samples were dried down directly in the deep-well plate and resuspended in MS loading buffer (2% ACN/0.3% TFA) prior to LC-MS analysis.

LC-MS analysis

For all samples, 1 μg of peptides were loaded onto an in-house packed 75 μm ID x 50 cm column packed with 1.9 μm C18 material (Dr Maisch, ReproSil Pur C18-AQ) with an Dionex UltiMate 3000 HPLC coupled to a

Q Exactive HF-X mass spectrometer. Peptides were eluted with a gradient of 5-30% ACN containing 0.1% FA over 90 min at 400 nL/min, and column temperature was maintained at 60°C with a column oven (Sonation).

All 26 mouse islet samples were run as unfractionated single-run samples, with the mass spectrometer operated in data-independent acquisition (DIA) mode. One full MS1 scan was acquired (scan range 350-1400 m/z, 3e6 AGC fill target; max IT 45 ms; 120,000 resolution), followed by 48 data-independent MS2 scans with 1 Th overlapping mass windows spanning from 350-975 m/z (isolation window 14 m/z; max IT 22 ms; first fixed mass 200 m/z; AGC fill target 1e5; 17,500 resolution; normalized collision energy 25).

To generate the fractionated DDA spectral libraries for each of the 6 strains, an identical LC setup was used as described above, with the following exception: peptides were eluted over a 240 min gradient. In addition the following MS settings were used: one full-MS1 scan (scan range 350-1400 m/z; 3e6 AGC fill target; max IT 20 ms; 60,000 resolution), followed by up to 15 MS2 scans (1.4 m/z isolation width; 17,500 resolution; 1e5 AGC fill target; 1e3 minimum AGC target max IT 25 ms; 100 m/z first fixed mass; normalized collision energy 25). Charge states 2-4 were selected for fragmentation, peptide match was set to preferred, exclude isotopes on and dynamic exclusion 30 s.

Data analysis – LC-MS/MS

To generate the islet proteome spectral library RAW data from fractionated pooled strain samples were processed using MaxQuant (v1.6.7.0) (Cox and Mann, 2008) using default settings, including enabling of LFQ, with minor changes: ''match between runs'' was enabled with a time window of 0.7 min to transfer identifications between adjacent fractions. Database searching was performed using the Andromeda search engine integrated into the MaxQuant environment, with searches performed against the mouse UniProt database (June 2019 release), concatenated with known contaminants and reversed sequences of all entries. Protein, peptide and site FDR thresholds in MaxQuant were each set to a maximum of 1%.

Prior to library-based analysis of the DIA data, RAW files were converted into htrms files using the htrms converter (Biognosys) with parameters set to default. The htrms files were analyzed with Spectronaut (version: 13.10.191212, Biognosys) using the MaxQuant-generated spectral libraries and default settings.

Metabolic Health Index

The Metabolic Health Index (MHI) was generated to incorporate both *in vivo* and *ex vivo* phenotypic measurements into a single metric by which individual mouse samples could be ranked. The following bias were assigned for *in vivo* measurements; incremental AUC: -1.2, fasting insulin: -1.0, fasting glucose: -0.9, fat mass: -0.8, and for *ex vivo* measurements; basal insulin secretion: -0.8, insulin content: -0.5, stimulated insulin secretion: 0.2. Increased fasting plasma glucose and impaired glucose tolerance are diagnostic criteria within the clinical setting (American Diabetes, 2011). Increased fat mass, fasting plasma insulin, and islet basal insulin secretion present as additional risk factors for clinical T2D diagnosis (Bays et al., 2007; Thomas et al., 2019). Insulin content as a surrogate of absolute insulin deficiency reflects clinical classification-peptide measurements in diabetes (Shields et al., 2012) and stages of beta-cell failure associated with T2D (Halban et al., 2014). Stimulated insulin secretion was slightly positively weighted to reflect increased capacity for beta-cell compensation, and clinically observed impaired insulin secretory responses in patients with increased T2D risk (Stumvoll et al., 2002).

Weighted gene Co-expression network analysis

Weighted gene co-expression network analysis (WGCNA) is a powerful tool for analyzing biological networks (Langfelder and Horvath, 2008). MetaNetwork (https://github.com/smith-chem-wisc/MetaNetwork), an R application for performing WGCNA was used to generate module memberships and identify eigenproteins. WGCNA uses the value of Pearson correlation to define a similarity matrix between gene *i* and gene *j*. The correlations matrix is transformed into a signed adjacency matrix by the equation $adjacency_{i,j} = (0.5 * (1 + corr(x_i x_j))^{\beta}$, using the adjacency function from the WGCNA package. The power, β, was selected to ensure scale free topology and was left at the default value of 12. Next, the Topological Overlap Matrix (TOM) was created from the adjacency matrix using the TOMsimilarity function, and the dissimilarity matrix was calculated. The dissimilarity TOM was used as distance measurements to perform hierarchical clustering on the proteins; the resulting dendrogram and the dissimilarity TOM were used to construct modules using the cuttreeDynamic function, with the deepSplit parameter set to

2, indicating medium cluster detection sensitivity. Eigenproteins for each module were calculated using the moduleEigengenes function. Modules were merged by calculating the distance between the modules using the Pearson correlation as the distance metric. Modules below a height of 0.25 (corresponding to an approximately 0.75 correlation coefficient) were merged, and the eigenproteins were re-calculated.

Phenotype-eigenprotein correlation was performed by taking the Pearson correlation between the module eigenprotein and the rank-normalized phenotype data using the cor function from the WGCNA package (Langfelder and Horvath, 2012). Correlations between the module eigenproteins and the categorical data were performed using the point-biserial correlation coefficient with chow given a value of 0 and high fat diet a value of 1.

Allez, GSEA, enrichment analyses

Gene Ontology (GO) Enrichment Analysis was performed using the enrich_shiny R application (https://github.com/lengning/Enrich_shiny), using the option for allez enrichment (Newton et al., 2007). Allez compares the frequency at which GO terms appear within a set of proteins to the frequency of the same GO terms in the gene universe and returns a standardized Z-score. For this analysis, the protein universe was defined as the entire set of proteins analyzed. All proteins were scored with either a 0 or 1, with the proteins inside the evaluated module receiving a 1, and proteins not belonging to the module receiving a 0. The allez function is used to calculate the Z-score, and adjusted p-values corresponding to the Z-score were calculated using the Benjamini-Hochberg's correction.

Seahorse islet respirometry

Islet respirometry (oxygen consumption rate, OCR) was performed using Seahorse XFp miniplates and a Seahorse XF HS Mini Analyzer (Seahorse Bioscience, Copenhagen, Denmark). For each strain, islets were isolated and 50 islets/well per individual mouse were seeded onto matrigel-coated plates and incubated overnight in islet media. Diabetic *db/db* mouse islets were cultured overnight at 20 mM glucose conditions to maintain *in vitro* hyperglycaemia. The day of the assay, islets were washed twice with KRBH and incubated in KRBH supplemented with 2.8 mM glucose without BSA (150 µl/well) at 37°C for 1h in non-CO_2 incubator. Islets were then assayed in XFp Analyzer. After 12 min equilibration period, oxygen consumption rate was measured with mix/wait/read cycles of 3/0/3 min. Following stabilization of baseline rates, compounds were injected sequentially to reach a final concentration of: 20 mM glucose, oligomycin (5µg/ml), FCCP (1 µM) and rotenone/antimycin A (5 µM) (Haythorne et al., 2019; Taddeo et al., 2018) to assess glucose-dependent respiration (calculated by baseline – glucose OCR), ATP-linked respiration (determined by glucose – oligomycin OCR), maximal respiration (calculated by FCCP – AntA/Rot OCR) and non-mitochondrial respiration respectively (equal to AntA/Rot OCR) Taddeo et al. (2018). Data are presented as O_2/min/50 islets.

QUANTIFICATION AND STATISTICAL ANALYSIS

Metabolic data analyses were performed using GraphPad Prism 8 software. Proteomics data was analyzed with Perseus software, version 1.6.12 (Tyanova et al., 2016) and RStudio version 1.4.1717 running R version 4.1.0. Islet proteome data was log2-transformed and normalized by median subtraction. Hierarchical clustering was performed with Euclidean distance metric and complete linkage.

Two-way ANOVA was used for strain and diet comparisons across different groups. ANOVA p-values were multiple hypothesis corrected with FDR (Benjamin-Hochberg) correction, and proteins with $q < 0.05$ reported. One-way ANOVA with Sidak's multiple-comparison post-test was used in respiratory OCR comparisons between strains with all islet groups $n = 3$, with statistical significance was set at adjusted $p < 0.05$. Data are expressed as mean ± S.E.M.

ADDITIONAL RESOURCES

Proteome data may be accessed online at https://www.kebedelab.com/islet-proteome-resource.